Journal of Thermal Analysis and Calorimetry (2019) 135:461–474
https://doi.org/10.1007/s10973-018-7356-y

Investigating the effect of connection type of a sintered porous fin through a channel on heat transfer and fluid flow

Mehrdad Mesgarpour[1] · Ali Heydari[2] · Seyfollah Saddodin[1]

Received: 16 January 2018 / Accepted: 4 May 2018 / Published online: 17 May 2018

Abstract

Extended surfaces represent one of practical approaches to enhance heat transfer. Based on the laws of conductive and convective heat transfer, an increase in the area across which the object is in contact with the fluid can increase heat transfer. Due to its special structure, porous media can be seen as suitable alternatives for extended surface applications. On this basis, this research investigates the effect of connection type of sintered porous fins on heat transfer and pressure drop in the fluid flow. Connection model of four- and six-contact sintered balls of constant dimensions was evaluated by means of CFD simulation in this research. To describe the problem further, surface analysis on the reference cube is presented. The results indicate that the six-contact model has more porosity than the four-contact in reference cube by 29.45%. It was further found that the six-contact model tends to increase convective heat transfer by 33%. Results of surface analysis show that the main reasons for the difference in heat transfer between the four- and six-contact models are porosity and the angle at which balls are arranged with another.

Keywords Sintered fin · Porosity · Connection type · Surface analysis

List of symbols

A	Surface area (m^2)
C_p	Specific heat (J kg K^{-1})
d_p	Ball diameter (m)
$D_{h,ch}$	The hydraulic diameter of the channel
G_k	Turbulence kinetic energy generated due to velocity (W)
G_B	Turbulence kinetic energy generated due to body force (W)
h	Heat transfer coefficient (W m^{-2} K)
H	Enthalpy (J)
K	Thermal conductivity (W m k^{-1})
k	Kinetic energy (J kg^{-1})
L	Fin length (m)
$\dot{m}$	Mass flow rate (kg s^{-1})
Nu	Nusselt number
P	Pressure (pa)
ΔP	Pressure drop (Pa)
$\dot{Q}$	Heat transfer (w)
Re	Reynolds number
S	Source term
T	Temperature (K)
U	Fluid velocity (m s^{-1})
Y_M	Turbulence density

Greek symbols

ε	Energy dissipation (J kg^{-1})
μ	Absolute viscosity (N s m^{-2})
η	Thermal efficiency
ρ	Density (kg m^{-3})
σ	Turbulent Prandtl number
θ	Dimensionless temperature

Subscripts

f	Fluid
s	Solid surface
w	Wall
$cond$	Conduction
$conv$	Convection
$total$	Total
$LMTD$	Logarithmic average of the temperature difference

✉ Ali Heydari
a.heydari@semnaniau.ac.ir

[1] Department of Mechanical Engineering, Semnan Branch, Islamic Azad University, Semnan, Iran

[2] Energy and Sustainable Development Research Center, Semnan Branch, Islamic Azad University, Semnan, P. O. Box: 35196-97951, Iran

in	Inlet
out	Outlet
fin	Related to fin
ave	Average
b	Base
i	Interface of solid and liquid

Introduction

According to Fourier's law, an increase in the fluid–solid contact area can be seen as a method for enhancing heat transfer. This can also be altered with changes in convective heat transfer coefficient or increasing temperature gradient. However, for many reasons and based on some limitations in manufacturing and operating conditions, the increase in contact surface area with extended surfaces has remained the best and the most cost-effective approach for heat transfer enhancement.

Alteration of shape and material represent examples of methods used to enhance fin performance. In a fin, heat is spread from the fin base via conductive heat transfer. Considering radiation equations and operating temperature of fins in most of engineering devices, convection imposes large contributions in their heat transfer [1]. A lot of researches were performed on extended surfaces, and some examples are given in references [2–8].

One way to extend the fin contact surface is utilizing the porous medium like metal sponge, perforated plates or sintered powder to construct a fin. Porous fins are applied to enhance the heat transfer in some critical systems such as cooling of electronic equipment and mirrors in powerful lasers, industrial furnaces, combustors, catalytic and chemical particle beds, solid matrix or micro-porous heat exchangers, phased-array radar systems, packed bed regenerators, fixed-bed nuclear propulsion systems, micro-thrusters, transpiration cooling, spacecraft thermal management systems, and many others. Morga [9] investigated the effect of thermal resistance within porous fins. Their results revealed that the fin arrangement and porosity impose large impacts on flow regime within and around the porous fins, which in turn affects temperature distribution. In another research, Writz [10] conducted a study on the cooling effect of porous fins to develop the concept of using porous medium for this case. The results revealed that provided spherical model which adopted in porous medium matrix, leads to minimize the pressure drop for a cooling flow. A numerical investigation of heat transfer in porous fin was undertaken by Jeng and Tzeng [11]. They showed that at lower Reynolds numbers, maximum Nusselt number occurs at stagnation point. But as Reynolds number increases, this point tends to be shifted toward downstream of the flow. Hamdan and Al-Nimr [12] investigated the effect of porous fin in a channel containing parallel arrangement. The results indicated that the highest Nusselt number in such a problem corresponds to the highest pumping power. It was further showed that for the porous medium in this channel, lower input pump pressure is needed compared to that of solid fins, leading to enhancement in efficiency. The wide spectrum of the applications of conventional and porous fins has led many researchers stepping in very special fields in their research activities. With the advancement of electronic systems which employ integrated circuits (ICs), numerous thermal problems have been raised. This concept comprises the base for the research by Lindstedt and Karvinen [13]. They could find an appropriate explanation for the relation between thermal conduction in the fin and the rate of heat flux from the fin to the surrounding fluid. One of the approaches for fin optimization is to study the rate of entropy generation in the fins. Bijan [14] suggested that in a system, with decreasing the rate of entropy generation, one can enhance the system efficiency. In 2017, Chen et al. [15] used this method to optimize needle-shaped fins. Recognizing variability of the fin dimensions, they suggested optimal geometrical properties for the fin. Their results indicated that for the optimization purpose, the most important factor is the aspect ratio of cross-sectional area to length. Moreover, with increasing the diameter-to-height ratio, the temperature distribution is changed.

Alshuraiaan and Khanafer [16] numerically investigated the effect of porous fin position on natural convection to find the optimum location. They evaluated the natural flow conditions for different Rayleigh numbers. Their results indicated that horizontal fins increase the heat transfer rate and average Nusselt number for different Rayleigh and Richardson numbers, while these parameters are reduced with vertical fins. Bilen et al. [17] experimentally studied heat transfer and pressure drop characteristics of aluminum porous fins in a rectangular channel in which the effect of gap heights and longitudinal fin pitches was evaluated on Nusselt number, heat transfer enhancement ratio and heat transfer performance. They found that the use of larger gap height over fins has a significant effect on the Nusselt number, while the longitudinal fin pitch has a negligible influence on it. An analytical analysis was performed by Kundu and Lee [18] to determine the maximum heat transfer of annular step porous fins on a cylindrical primary surface. A comparison between porous and solid fins was done for an equal mass of fins, and the results showed that it is a profitable design aspect for selecting the porous condition in annular configuration. Siavashi et al. [19] numerically analyzed natural convection of Cu-water nanofluid in a cavity with an array of porous fins to investigate the effects of the fins number and their length

on heat transfer enhancement and entropy generation. Their results showed that adding porous fins with a high Darcy number improves heat transfer, while fins with a low Darcy number lead to poor convection and low Nusselt number. Ghalambaz et al. [20] numerically investigated the effect of inclined thin local thermal non-equilibrium porous fin on laminar free convection flow and heat transfer of a nanofluid in an enclosure. They found that the average Nusselt number is an increasing function of Ra, Pr and Da numbers and porosity and heat transfer shows a different behavior for different values of fin angles and lengths.

Despite various advantages offered by porous media, it has been always utilized based on approximations because of its probabilistic (stochastic) structure and texture. In other words, in theory, porous media is considered as a uniform body, so that a uniform pressure drop would occur within them. This is while, in reality, this media possess stochastic characteristics. On the other hand, besides heat transfer problems, strength issues are among uncertain topics in porous media. Engineered porous media is a kind of real porous media in which the construction of the holes and cavities can be manually changed, and the porosity and permeability can be controlled near high-temperature zones. For numerical simulation, Navier–Stokes equations are solved directly without approximate models and consequently viscous/inertia resistances are modeled without mediators. This kind of the porous medium can be constructed by some process like sintering, machining and drilling. In the present research, introducing a porous structure set in some special arrangement, a new variant of porous media is presented under the general name of *engineered porous media* [21].

Jiang et al. [22] experimentally investigated the effects of fluid velocity, particle diameter, type of porous media (sintered or non-sintered), and fluid properties on convection heat transfer in a porous plate channels. They showed that the convection heat transfer of the sintered porous plate channel was more intense than in the non-sintered one due to the reduced thermal contact resistance and the reduced porosity, especially for air. Also, their results indicated that the effective thermal conductivity of the sintered porous media was found to be much higher than for non-sintered one due to the improved thermal contact caused by the sintering process. Later, Jiang and Lu [23] numerically analyzed sintered balls in a channel to investigate heat transfer in such balls. They observed that with reducing the size of the spheres, heat transfer increases. Chuan et al. [24] studied a micro-channel created with a bed of metal balls to investigate such an environment and the effect of this porous bed on increasing heat transfer. They found drag coefficient reduction in a channel of this new geometry. They further understood that the design and type of the developed porous environment in the channel bed is directly related to the drag force established in the channel. Zhong et al. [25] determined the pressure drop for air flow through sintered metal porous media using a modified Ergun equation. They found that compressibility effect can intensify the pressure drop and there exists a range of transitional diameters, within which the wall effect on the pressure drop would become extremely uncertain. Huang et al. [26] performed an experimental research on transpiration cooling with phase change for sintered bronze porous plates in a wind tunnel. The results indicated that the average cooling efficiency and maximum temperature enhanced due to the reduction in the particle diameter of the sintered bronze porous plate.

In this paper, as the novelty of the research, the effects of connection type (vertical and diagonal) on heat transfer and pressure drop are investigated. The importance of the research corresponds to thermal and flow behavior of engineered porous fins with different type of particle connections. In vertical connection, each ball (except edge balls) is in contact with four neighboring balls. While in diagonal connection, each ball is in contact with six neighboring balls. This is the basis on which heat transfer and pressure drop are investigated in these fins. For this purpose, the fin is situated in a channel of known dimensions in perpendicular to the flow direction, and effects of Reynolds number, heat flux, and base temperature on thermal and flowing behaviors of the fin are investigated. The fin dimensions (length and width) in six-contact case are exactly the same as those for the four-contact type, so as to be able to compare fins in surface area, volume, and convection coefficient. In addition, in the present research, surface analysis of a given control volume is presented based on the four- and six-contact models.

Governing equations

According to energy balance in a control volume in a fin by neglecting radiation heat transfer (due to low temperatures in this work), we have:

$$\dot{Q}_{\text{total}} = \dot{Q}_{\text{cond}} + \dot{Q}_{\text{conv}} \tag{1}$$

where $\dot{Q}_{\text{cond}}$ and $\dot{Q}_{\text{conv}}$ are the amount of heat transferred via thermal conduction and convection, respectively, for which we have:

$$\begin{aligned} \dot{Q}_{\text{conv}} &= C_{\text{p}}\dot{m}(T_{\text{out}} - T_{\text{in}}) \\ \dot{Q}_{\text{cond}} &= -KA\nabla T \end{aligned} \tag{2}$$

where $\dot{m}$ is mass flow rate of the fluid, T_{out} is output fluid temperature, and K is the conductive heat transfer coefficient. The convection equation can also be obtained based on the fin base temperature.

$$\dot{Q}_{\text{conv}} = h_{\text{av}} A_{\text{s}} \left[T_{\text{b}} - \left(\frac{T_{\text{in}} - T_{\text{out}}}{2} \right) \right] \tag{3}$$

where h_{av} is average convective heat transfer coefficient, T_{b} is the base temperature of the surface, and A_{s} is the side area of the fin. In convective heat transfer, a major objective of each experiment and numerical analysis is to find heat transfer coefficient. For this purpose, average convective heat transfer coefficient is defined as follows:

$$h = \frac{Q_{\text{ave}}}{A_{\text{s}} \Delta T_{\text{LMTD}}} \tag{4}$$

$$\Delta T_{\text{LMTD}} = \left[\frac{\left(T_{\text{s,ave}} - T_{\text{f,ave,in}} \right)}{\ln\left(\frac{T_{\text{s,ave}} - T_{\text{f,ave,in}}}{T_{\text{s,ave}} - T_{\text{f,ave,out}}} \right)} \right] - \left[\frac{\left(T_{\text{s,ave}} - T_{\text{f,ave,out}} \right)}{\ln\left(\frac{T_{\text{s,ave}} - T_{\text{f,ave,in}}}{T_{\text{s,ave}} - T_{\text{f,ave,out}}} \right)} \right] \tag{5}$$

In the above equation, which is expressed in term of logarithmic temperature gradient, $T_{\text{s, ave}}$ is average surface temperature, $T_{\text{f, ave, in}}$ is average input temperature into the system, and $T_{\text{f, ave, out}}$ is average output temperature of the system. Moreover, equations of continuity, momentum, and energy in the fluid around a solid object are as follows:

$$\begin{aligned} &\nabla \cdot (\boldsymbol{\rho U}) = 0 \\ &\nabla \cdot (\rho UU) = -\nabla P + \nabla \cdot \left(\mu \left(\nabla U - \frac{2}{3} \nabla \cdot UI \right) \right) \\ &\nabla \cdot (\boldsymbol{\rho UH}) = \nabla \cdot (\boldsymbol{K}_{\mathbf{f}} \nabla \boldsymbol{T}_{\mathbf{f}}) \end{aligned} \tag{6}$$

It should be noted that in the present work, the geometry of the porous medium is modeled directly by considering the joined rigid balls, and flow analysis between the balls is also performed without activating the porous medium and applying its assumptions in the governing equations. In addition, the viscosity and inertial resistance of the porous medium will be calculated automatically by modeling the fluid flow through the balls. Therefore, it is not necessary to apply porosity in the governing equations. To present the results, it is convenient to define some dimensionless parameters. In this way, the results are not depending on boundary conditions or dimensions of the problem. These dimensionless parameters can be defined as follows:

$$\theta = \frac{T_{\text{s,ave}} - T_{\text{f,ave,in}}}{T_{\text{b}} - T_{\text{f,ave,in}}}; \quad \text{Re} = \frac{\rho U_{\text{in}} D_{\text{h,ch}}}{\mu}, \quad \text{Nu} = \frac{hL}{K_{\text{f}}} \tag{7}$$

where $D_{\text{h,ch}}$ is the hydraulic diameter of the channel and L is the fin length. The fin efficiency can be obtained from the following equation in which q_{fin} is heat transfer from the fin, h is convection heat transfer coefficient, and A_{fin} is contact surface of fin and fluid:

$$\eta = \frac{q_{\text{fin}}}{h A_{\text{fin}} (T_{\text{ave}} - T_{\text{b}})} \tag{8}$$

For numerical solution of heat transfer and fluid mechanics equations, the k–ε turbulence model was used in the present research. This model is considered as follows:

$$\begin{aligned} \frac{\partial}{\partial x_{\text{i}}} (\rho k u_{\text{i}}) + \frac{\partial}{\partial t} (\rho k) = \frac{\partial}{\partial x_{\text{j}}} \left(\left(\mu + \frac{\mu_{\text{t}}}{\sigma_{\text{k}}} \right) \frac{\partial k}{\partial x_{\text{j}}} \right) + G_{\text{K}} + G_{\text{b}} \\ - \rho\varepsilon - Y_{\text{M}} + S_{\text{K}} \end{aligned} \tag{9}$$

$$\begin{aligned} \frac{\partial}{\partial x_{\text{i}}} (\rho \varepsilon u_{\text{i}}) + \frac{\partial}{\partial t} (\rho \varepsilon) = \frac{\partial}{\partial x_{\text{j}}} \left(\left(\mu + \frac{\mu_{\text{t}}}{\sigma_{\varepsilon}} \right) \frac{\partial \varepsilon}{\partial x_{\text{j}}} \right) \\ + C_{1\varepsilon} \frac{\varepsilon}{k} (G_{\text{K}} + C_{3\varepsilon} G_{\text{b}}) + C_{2\varepsilon} \rho \frac{\varepsilon^2}{k} \\ + S_{\varepsilon} \end{aligned} \tag{10}$$

In the above-mentioned equations, G_{k} represents the amount of turbulence kinetic energy generated due to velocity gradient, G_{b} is the amount of turbulence kinetic energy generated due to buoyancy forces, and Y_{M} denotes the portion of fluctuations in turbulence density out of total energy dissipation. This parameter is also known as turbulence density. C is a constant, and σ is turbulent Prandtl number. Finally, S is the source term [27]. In this case, the boundary conditions are very important in the interface between the fluid and solid. So we have:

$$\begin{aligned} &\boldsymbol{K}_{\mathbf{f}} \nabla \boldsymbol{T}_{(\mathbf{fi})} = \boldsymbol{K}_{\mathbf{s}} \nabla \boldsymbol{T}_{(\mathbf{si})} \\ &T_{(\text{fi})} = T_{(\text{si})} \end{aligned} \tag{11}$$

Problem definition

Geometry

To investigate the effect of connection type on convective heat transfer in sintered fins, according to Fig. 1, fins were designed in two cases. In the first case, which was considered as the four-contact model, the balls are orthogonally connected to one another, with each row placed exactly on top of the lower row. Moreover, in the six-contact case, according to the figure, the balls contacts diagonally with each other. Since two models are designed with identical dimensions (in terms of length, width, and ball diameter), thus in six-contact model, one and a half rows are added to the fin in comparison with four-contact case. According to sintering process, the balls of the porous fins seamlessly integrated together and almost there is no difference between the material structure of connection zones and other parts of the fin. In the numerical simulation, it is tried to model the balls connections and other parts of the fin uniformly. It should be acknowledged that the geometry of the problem has been designed with SolidWorks 2018 software.

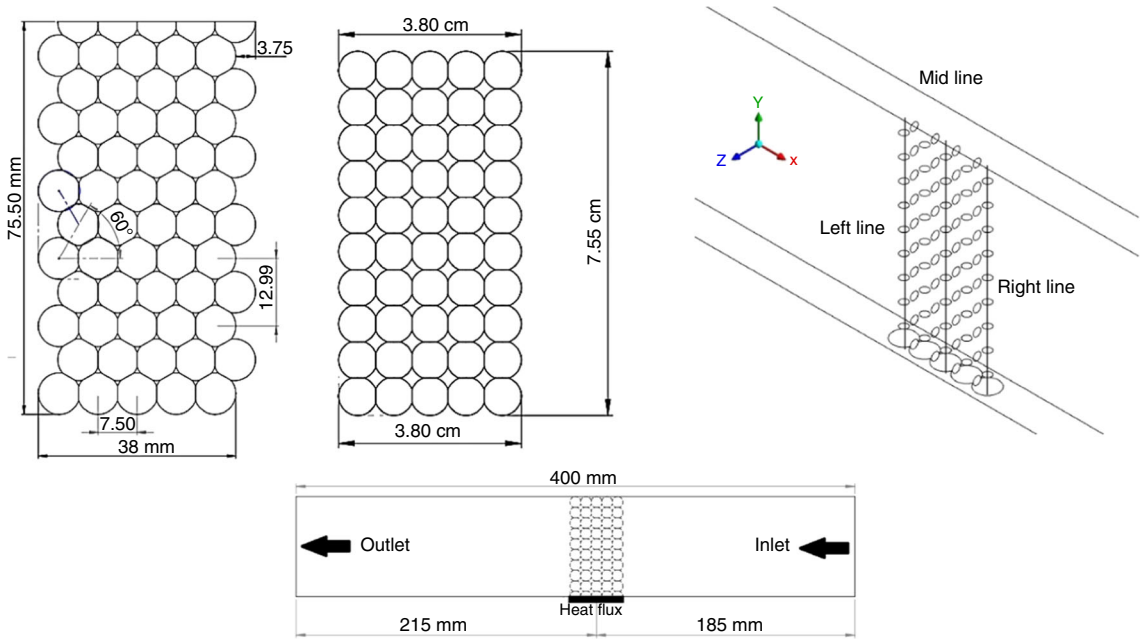

Fig. 1 Fin and channel dimensions and an overview of the measurement lines of the variables

Moreover, according to Fig. 1, the fins were placed in a rectangular channel in which the fluid streams into the channel from the input and leaves it from the marked output. The dimensions of the channel are illustrated in this figure. To calculate the values, according to Fig. 1, three lines were drawn: left, middle, and right lines. It should be noted that the flow direction is along reverse x direction, with the coordinate system defined as shown.

Boundary conditions

To achieve a solution of the governing equations, numerical methods require the known boundary conditions of the problem. As such, boundary conditions were defined for the considered problem in four- and six-contact cases with heat flux at fin base and input air temperature taken to be 300 K. Input velocities were in the range 1–3 m s^{-1} (at 0.5 m s^{-1} increment steps). Moreover, to consider the effect of heat flux and fin base temperature, different values of input heat flux to the fin base (5000, 7500 and 10,000 W m^{-2}) and base temperatures (325, 350, 400, and 450 K) were studied.

Numerical aspects

The 3D heat transfer problem was solved using the CFD software ANSYS/FLUENT 18.2. The fluid flow regimes in the porous media ranged from laminar to turbulent flow. Thus, the $k-\varepsilon$ turbulence model was used in the present research to simulate the turbulent flow. To couple the pressure and velocities, the SIMPLE algorithm was employed. The second-order upwind was applied in the momentum, energy, turbulent kinetic energy, and turbulent energy dissipation equations.

Mesh study

Figure 2 shows the effect of changes in the number and size of mesh on the obtained maximum temperature on the fin surface. As can be seen from the figure, no significant changes in maximum temperature were observed with meshes composed of more than 400,000 cells, so that the

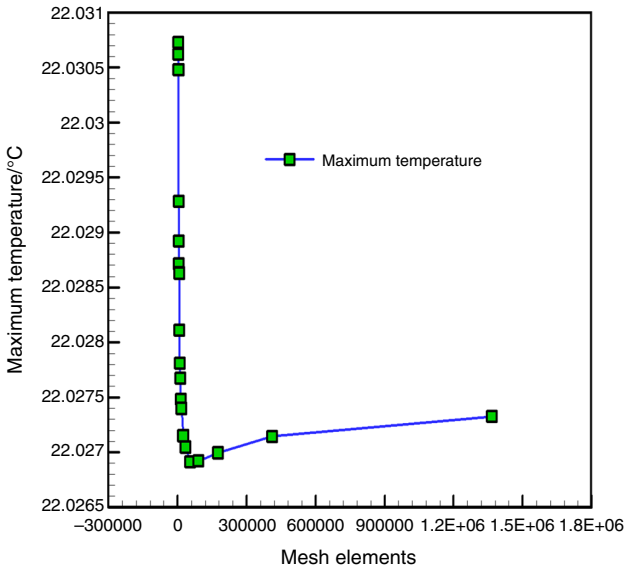

Fig. 2 Independence diagram of the mesh for six-contact fins

400,000 can be selected as optimal mesh count. Further, in the present research, fully developed polyhedral meshing was adopted to study the considered problem. It can be referred to its optimal structure as the most important characteristics of this type of meshing. This structure is based on unstructured triangular network-based optimization algorithm. In software analysis of a simultaneous convective–conductive heat transfer phenomenon, mesh size is important for determining fluid temperature, particularly close to the solid surface. A sample of the selected mesh can be observed in Fig. 3.

Validation

To validate the obtained results, first of all, the model of balls was evaluated with the help of Jiang and Lu [23]. In this case, after substituting the conditions declared in Ref. [23] into the solution approach and comparing the results, the obtained data were validated. According to Fig. 4, for the amount of heat transfer along the fin, it is observed that at maximum heat transfer, the obtained result is 3.18% different from the reported value in Ref. [23].

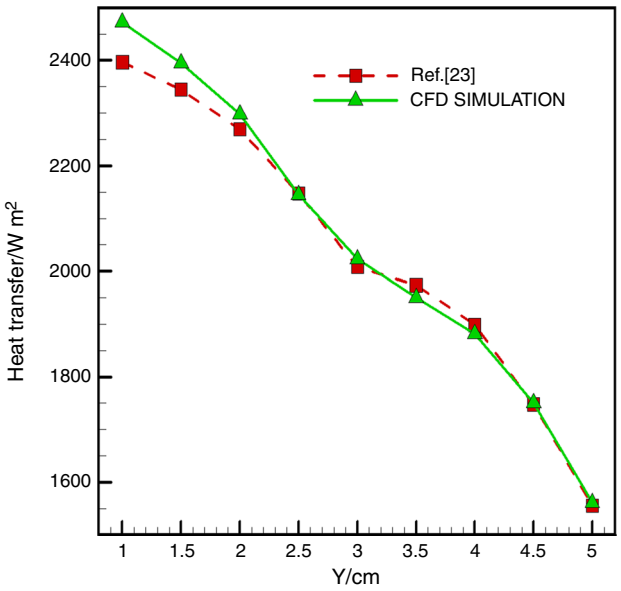

Fig. 4 Comparing obtained heat transfer for four-contact model of CFD simulation and Jiang and Lu [23]. (d_p (ball diameter) = 1.7 mm, U_{in} = 11.4 mm s^{-1}, $T_{f\ in}$ = 300.0 K, q_w (base heat flux) = 31,730 W m^{-2})

Results and discussion

As was mentioned in previous section, the present research studies heat transfer and pressure drop in sintered fins. For this purpose, first of all, surface analysis was undertaken on the two modes presented: four-contact and six-contact models. Next, flow analysis was conducted for the sintered fin connected via four and six contacts with a final comparison between the two cases. At first, a surface analysis has been performed to evaluate the body differences of two models. Then the effects of variation in Reynolds number and thermal boundary conditions of the fin base are investigated on thermal performance of the fin.

Surface analysis

To investigate and analyze contact area of the balls and the area of the fin, firstly, SolidWorks Software was utilized to draw 3D model of the balls. Afterward, Geomagic Control Software was used to analyze surfaces, angles, and other geometrical characteristics. The four- and six-contact models for the considered fins differed in not only the number of contacts, but also surface area and volume of the fins. In this section, by surface analysis and investigation of other effective parameters, the four- and six-contact fins were compared. According to Fig. 5, the reference blocks for the four- and six- contact cases were considered with the demonstrated properties. As is evident on the figure, the four-contact block contains one full sphere along with three fragmented spheres.

In this figure, the porosity for the four-contact case was calculated to be 58.88%. In other words, this model contains 41.12% of occupied space. Similarly, for the six-contact case (Fig. 5b), the porosity was calculated to be 33.88%, i.e., about 66.11% of the model was occupied. Obviously, the fin is more compact in the six-contact case rather than the four-contact one. Moreover, surface deviation and analysis results for the four- and six-contact cases

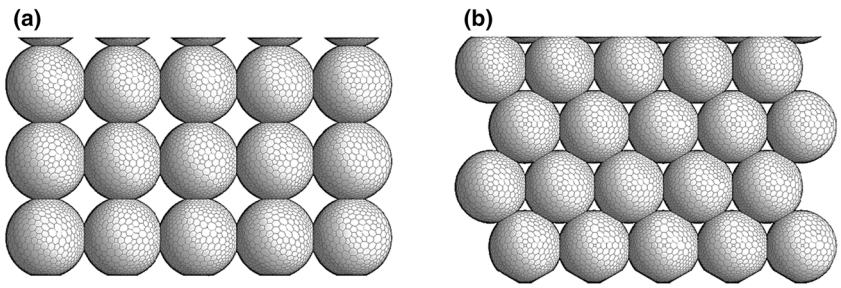

Fig. 3 Generated network for **a** four-contact model and **b** six-contact model

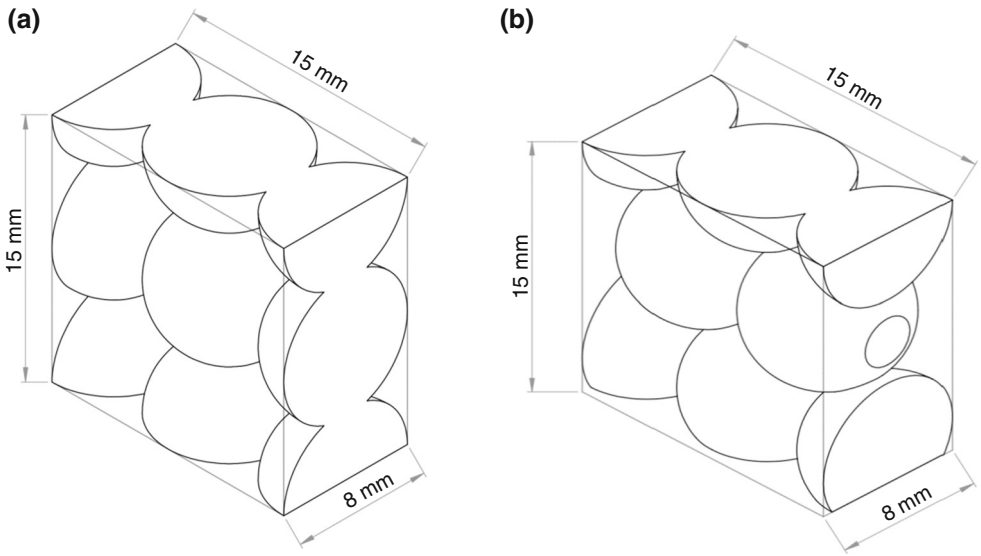

Fig. 5 Reference block for **a** four-contact, **b** six-contact models

are reported in Tables 1 and 2. The important point in these tables is the contact surface area in the four- and six-contact cases. While the surface for the four-contact case is 1096 mm^2, it is about 1058 mm^2 for the six-contact case. In other words, the four-contact case is associated with larger surface area per reference volume.

Another point of difference between the four- and six-contact cases is the surface normal vectors. In the four-contact case, all of the balls are orthogonally arranged with respect to one another. This is while, in the six-contact case, since the balls are connected at 60° angle to the upper balls in the upper row, the contact zone consists of various angles. In Fig. 6, one can see these deviations.

Table 2 Four-contact surface feature

Total surface area analyzed	10.96/cm^2
Critical surface area (% of analyzed area)	2.48/cm^2 (22.62%)
Maximum deviation from target thickness	0.25/cm
Average weighted thickness on critical area	0.21/cm
Average weighted thickness on analyzed area	0.46/cm
Number of critical faces	12 Face/s
Number of critical features	2
Minimum thickness on analyzed area	0.05/cm
Maximum thickness on analyzed area	1.5/cm

Comparison of performance for four- and six-contact fins

In the first step of investigating, thermal performance of the fins is evaluated. Figure 7 shows the plot of average dimensionless temperature for the three lines drawn in Fig. 1 at different Reynolds numbers (based on hydraulic diameter of channel) in the four-contact (a) and six-contact (b) models. The fluid at initial temperature has the highest heat transfer as it hits the first row of balls due to the largest temperature difference. Thus, the average temperature is lower in the row at leading edge of the fins than that of other rows. As the distance from the leading edge increases, the increase in fluid temperature leads to lower temperature difference between the surface and the object, thereby decreasing heat transfer rate and enhancement surface temperatures on the fin. With increasing the value of Reynolds number of the flow, due to increased flow

Table 1 Six-contact surface feature

Total surface area analyzed	1058.87/mm^2
Critical surface area (% of analyzed area)	115.32/mm^2 (10.89%)
Maximum deviation from target thickness	3/mm
Average weighted thickness on critical area	2.06/mm
Average weighted thickness on analyzed area	6.37/mm
Number of critical faces	10 Face/s
Number of critical features	2
Minimum thickness on analyzed area	0/mm
Maximum thickness on analyzed area	17.05/mm

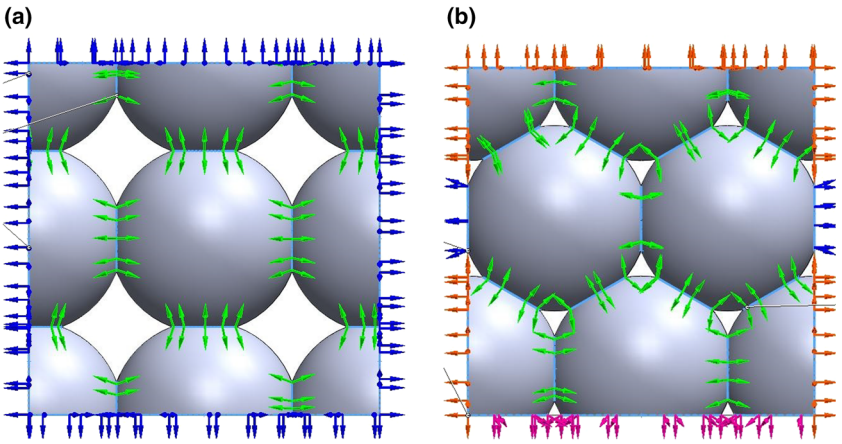

Fig. 6 Connection angles for **a** the four-contact model, **b** the six-contact model

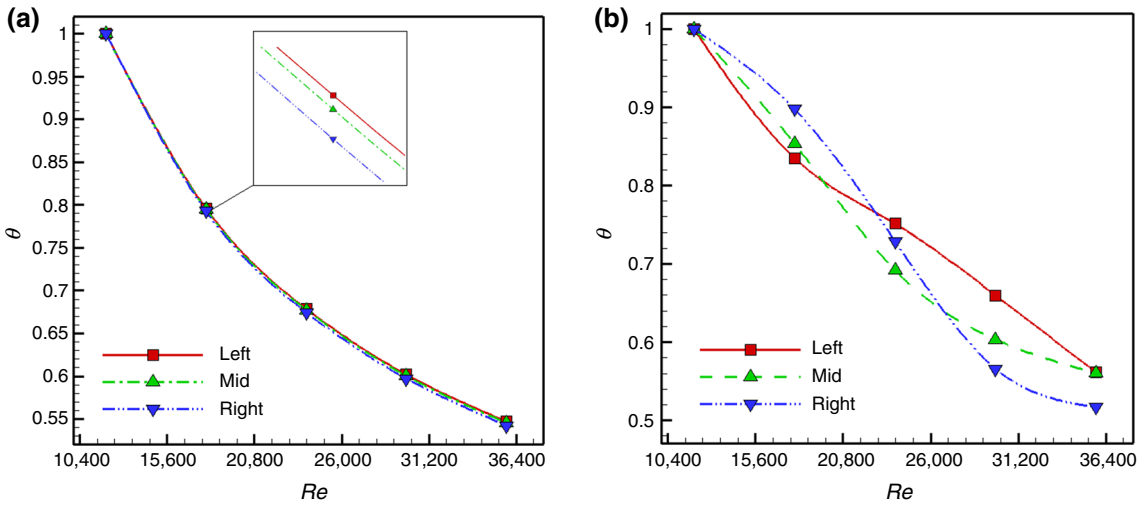

Fig. 7 Distribution of average dimensionless temperature with different Reynolds at heat flux of 5000 W for **a** four-contact and **b** six-contact models

velocity, surface temperature follows the same non-uniformly decreasing trend along all three lines, so that further decrease is seen in temperature at lower Reynolds numbers. On the other word, decreasing slope of temperature with increasing Reynolds number is higher in lower Reynolds numbers. This can be justified by the relation between Nusselt and Reynolds numbers. For four-contact model, the average dimensionless temperature on all three lines is approximately similar but for six-contact case the temperature distribution is related to Reynolds number. In low Reynolds numbers, the average dimensionless temperature at leading edge of six-contact fin is more than trailing edge while for high Reynolds numbers it reverses.

For the six-contact case, similar to the case with four contacts, the heat transfer between the fin and fluid is the most significant issue. It should be considered that in this analysis, the six-contact fin was designed to the same dimensions as those of the four-contact fin. That is, height and width of the six-contact fin were the same as those of the four-contact one. Since the balls are connected at 60° angle to one another in the six-contact case, thus, at the same length, the six-contact fin has 1.5 rows more than that of the four-contact one. This can be discussed from multiple points of view. The first thing to discuss on is the added surface area by the 1.5 rows of balls in the six-contact arrangement, and the second topic for discussion is the porosity percentage. These will highlight the effect of passing fluid and variations of its parameters. As was shown in the surface analysis section, when it comes to surface area, the six-contact fin tends to provide smaller fin-fluid contact area than that of the four-contact one in the reference block. However, due to the presence of an additional row, this conclusion is altered. Accordingly, taking into account the additional row, total surface area of the six-contact fin exceeds that of the four-contact one. On the other hand, porosity percentage of the six-contact case

is lower than that of the four-contact one. On this basis, the temperature distribution of the six-contact fin is different with four-contact one.

As was explained in the section on surface analysis, the fluid passing through the rows of four-contact balls will regularly hit horizontal and vertical arrangements of the fins. This is while, arrangement of the six-contact fins generate a different path at 60° for the fluid flow. This path along with differences in contact area and porosity percentage ends up with different heat transfer coefficients for the two fins.

Figure 8 shows the average Nusselt number for the four- and six-contact fins at different values of Reynolds number. The results indicate that at different Reynolds numbers, the six-contact fin provides higher Nusselt number than that of four-contact case (about 4.36%). The reason is the diagonal connection of balls and their non-homogeneous layout which leads to higher turbulence of the flow passing around the fin. In contrast, according to Fig. 9, the results indicate that in the six-contact fin, with increasing the Reynolds number, larger dimensionless pressure drop ($\gamma = \left(\frac{\Delta P_{ave} \Delta V_{ave}}{P_{in} V_{in}}\right)$) occurs with variations of input Reynolds number, as compared to the four-contact case. Of the most important causes of this situation, one can refer to the lower porosity in the six-contact case and different arrangement of the balls in the four- and six-contact fins. In the section on surface analysis, it was indicated that six-contact balls connection increases contact surface per constant length (due to the added row of balls), and also results in higher pressure drop due to higher flow turbulence due to non-homogeneous balls layout.

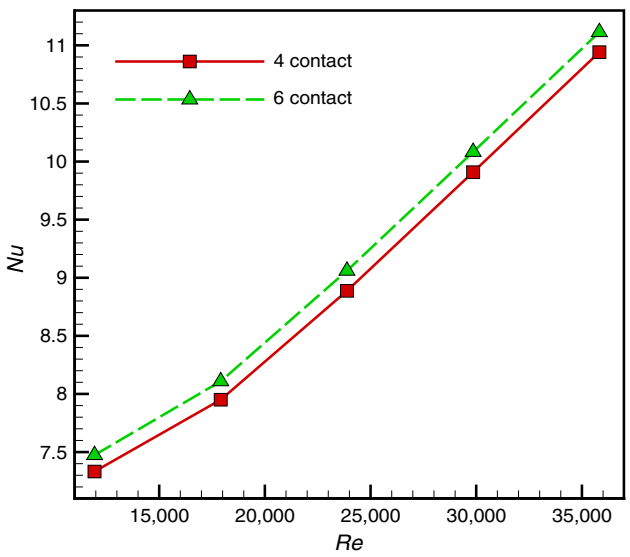

Fig. 8 Comparison of the average Nusselt number for fins in four- and six-contact modes based on Reynolds number changes at heat flux of 5000 W

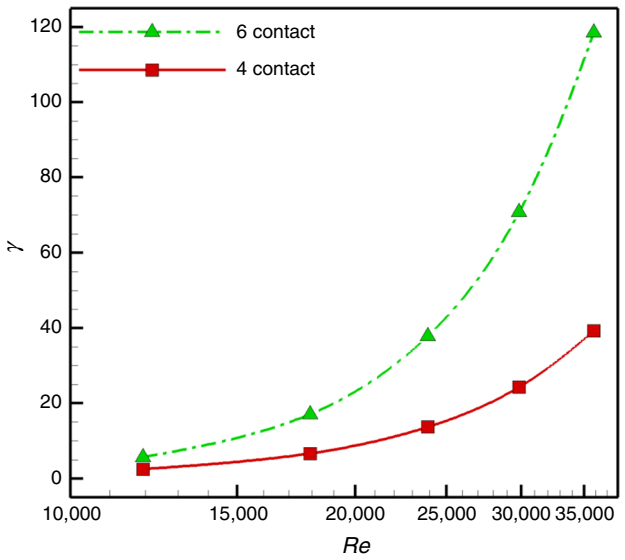

Fig. 9 Comparison of dimensionless pressure drop for fins in four- and six-contact modes based on changes in Reynolds number at heat flux of 5000 W

In Fig. 10, distribution of average dimensionless temperature over the entire fin is shown at flow velocity of 2.5 m s^{-1} for two boundary conditions at the base of the fin (325 K constant base temperature (a) and 5000 W constant base thermal heat flux (b)). Considering this figure, it is evident that at a given constant heat flux from the fin base, the average dimensionless temperature is varied in a higher range in comparison with the case of constant temperature at the base. Meanwhile, the temperature distribution of four- and six- contact fin for the case of constant temperature at the base is the same in 35% first part of the fin (on base side). This phenomenon indicates that for constant temperature at the base, the ball arrangement on base side is effect less on temperature distribution. But for the rest of the fin, the temperature of six-contact fin is lower than four-contact one. If constant heat flux is selected as the boundary condition of the fin base, the temperature of six-contact fin is lower than four-contact one for entire fin. The reason of this observation is related to the higher heat transfer rate due to higher fin surface (with the same dimensions) of six-contact in comparison with four-contact (as was mentioned in section of surface analysis). Due to approximately similar thermal boundary layers on the base side of the four- and six-contact cases, output heat fluxes of the four- and six-contact models were identical near the base where the temperature distributions were exactly the same. However, as one moves farther from the base where the effect of the thermal boundary layer is eliminated, the temperature difference between these two cases is more highlighted.

The effect of higher inlet velocity (10 m s^{-1}) on the average dimensionless temperature distribution for fins in

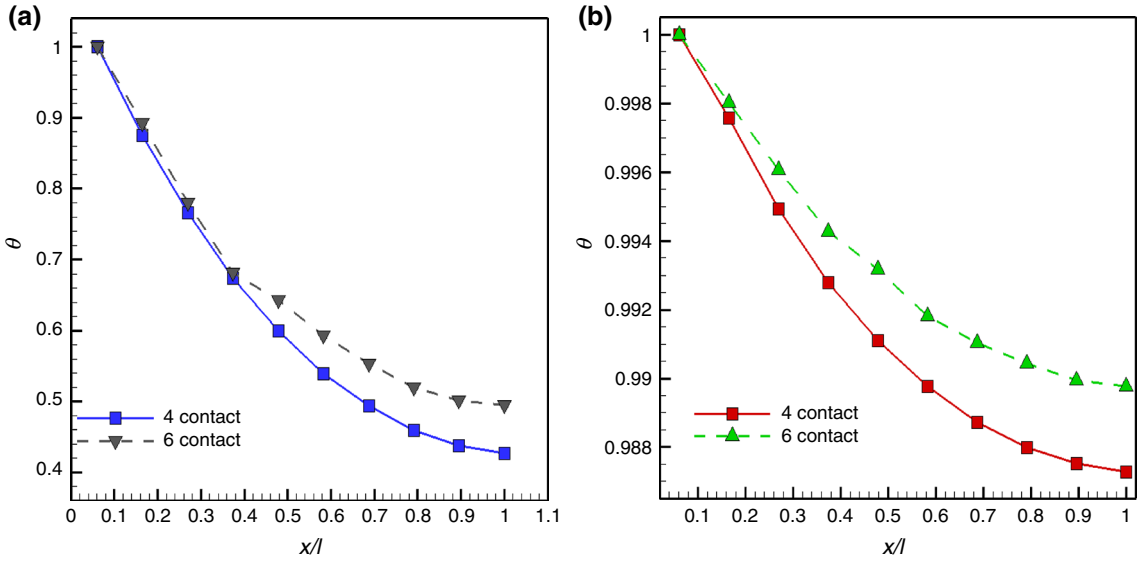

Fig. 10 Comparison diagram of the average dimensionless temperature distribution for fins in four- and six-contact modes at 2.5 m s^{-1} for different base thermal condition **a** 325 K constant base temperature, **b** 5000 W constant base thermal heat flux

four- and six-contact modes for 325 K constant base temperature (a) and 5000 W constant base thermal heat flux (b) is indicated in Fig. 11. It can be observed that for higher inlet velocity there is a little difference between temperature distributions of four- and six-contact cases.

In Fig. 12, effects of different constant temperature at fin base on the average Nusselt numbers for four- and six-contact fins are demonstrated for two inlet velocities. The horizontal axis is defined as the ratio of average fin temperature to base fin temperature. For low inlet velocity, the average Nusselt number is higher in the four-contact case rather than the six-contact one. This can be justified by the laminar nature of the flow regime. At lower velocities, due to the balls layout, the generated vortexes (and turbulence) behind the balls in six-contact fin are less than the four-contact one and lower heat transfer coefficient and Nusselt numbers are obtained. However, with increasing the flow velocity, the created vortexes behind the balls of six-contact fin are stronger which consequently increases the flow turbulence in this zone. This turbulence increases convective heat transfer coefficient dramatically, as compared to that of the four-contact case. Consequently Nusselt number of six-contact fin is obtained much more than four-contact one. Another result indicates that by increasing the base temperature of the fin the Nusselt number is decreased. This fact can be explained that by increasing the base

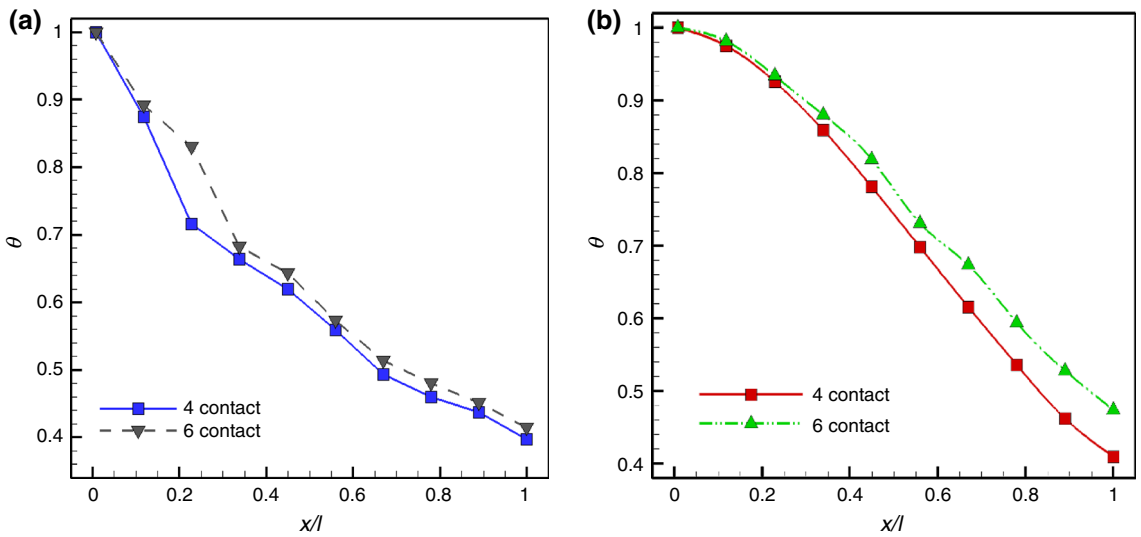

Fig. 11 Comparison diagram of the average dimensionless temperature distribution for fins in four- and six-contact modes at 10 m s^{-1} for different base thermal condition **a** 325 K constant base temperature, **b** 5000 W constant base thermal heat flux

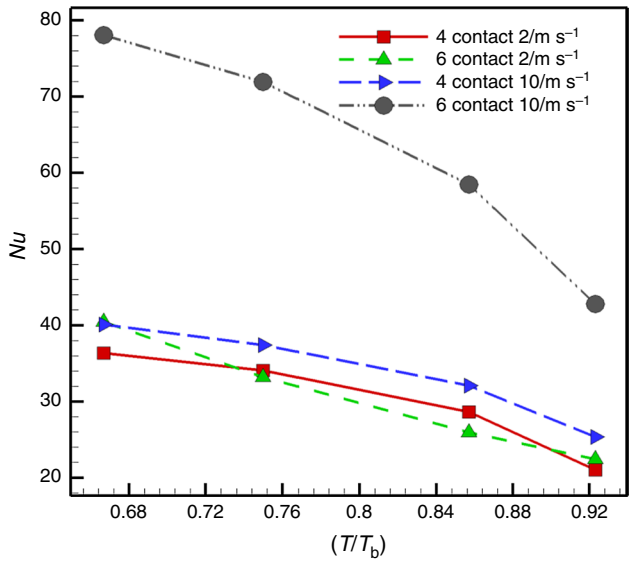

Fig. 12 Comparison diagram of the average Nusselt number for fins in four- and six-contact modes at 2.5 and 10 m s^{-1} for different base temperatures 325, 350, 400 and 450 K

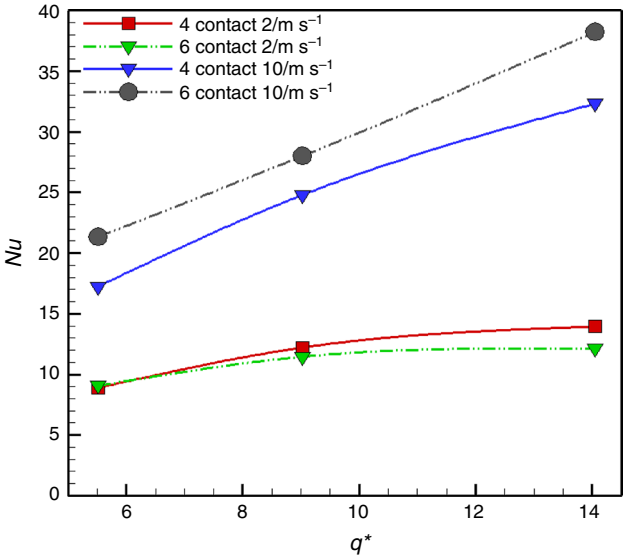

Fig. 13 Comparison diagram of the average Nusselt number for fins in four- and six-contact modes at 2.5 and 10 m s^{-1} for different base heat fluxes 5000, 7500 and 10,000 W

temperature, the average temperature of the fin will be enhanced and the temperature difference between solid and fluid will be reduced. Thus, heat transfer rate, convection heat transfer coefficient and consequently Nusselt number are reduced.

According to Fig. 13, for two inlet velocities, the effect of different constant heat fluxes at fin base on the average Nusselt number is demonstrated for four- and six-contact fins. The horizontal axis is defined as the dimensionless heat flux as $q^* = \frac{q_{\text{fin}}}{hA_b\left(T_b - T_{f,\text{ave,in}}\right)}$. The results show that for low inlet velocity, the Nusselt number for four- and six-contact modes is close to each other especially for lower heat flux in the base of the fin. For high inlet velocity, the Nusselt number of six-contact fin is obtained higher than four-contact one. Meanwhile, by enhancement in the base heat flux of the fin, the Nusselt number is increased. The reason is related to increasing heat transfer rate from the fin due to enhancement in fin base heat flux. Consequently convection heat transfer coefficient and Nusselt number will be increased.

The effect of Reynolds number on the fin efficiency for four- and six-contact modes for 325 K constant base temperature is illustrated in Fig. 14. As can be seen in this figure, increasing in Reynolds number leads to enhancement in fin efficiency for both four- and six-contact cases. As an important result, this diagram shows that the fin efficiency of six-contact case is higher than four-contact one. By averaging the Nusselt number in the range of Reynolds variation, it can be observed that six-contact mode increases the Nusselt number 3.2% higher than four-contact one.

Figure 15 demonstrates fin temperature contours for the four- and six-contact cases at different heat fluxes and flow velocities of 2.5 and 10 m s^{-1}. As is evident from the figure, with increasing the flow velocity, the thermal boundary layer and thermal diffusion inside the fin are decreased due to enhancement in convective heat transfer and larger share of heat transfer is carried out by the fluid. Besides, temperature variations were more intensive in the four-contact case than that in the six-contact case, at both lower and higher flow velocities. For instance, at a heat flux of 15,000 W and a flow velocity of 2.5 m s^{-1}, the contour

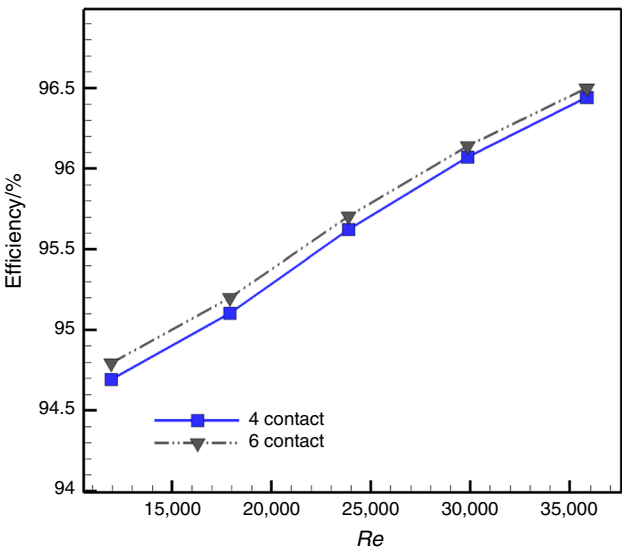

Fig. 14 Comparison of the fin efficiency in terms of Reynolds number for four- and six-contact modes for 325 K constant base temperature

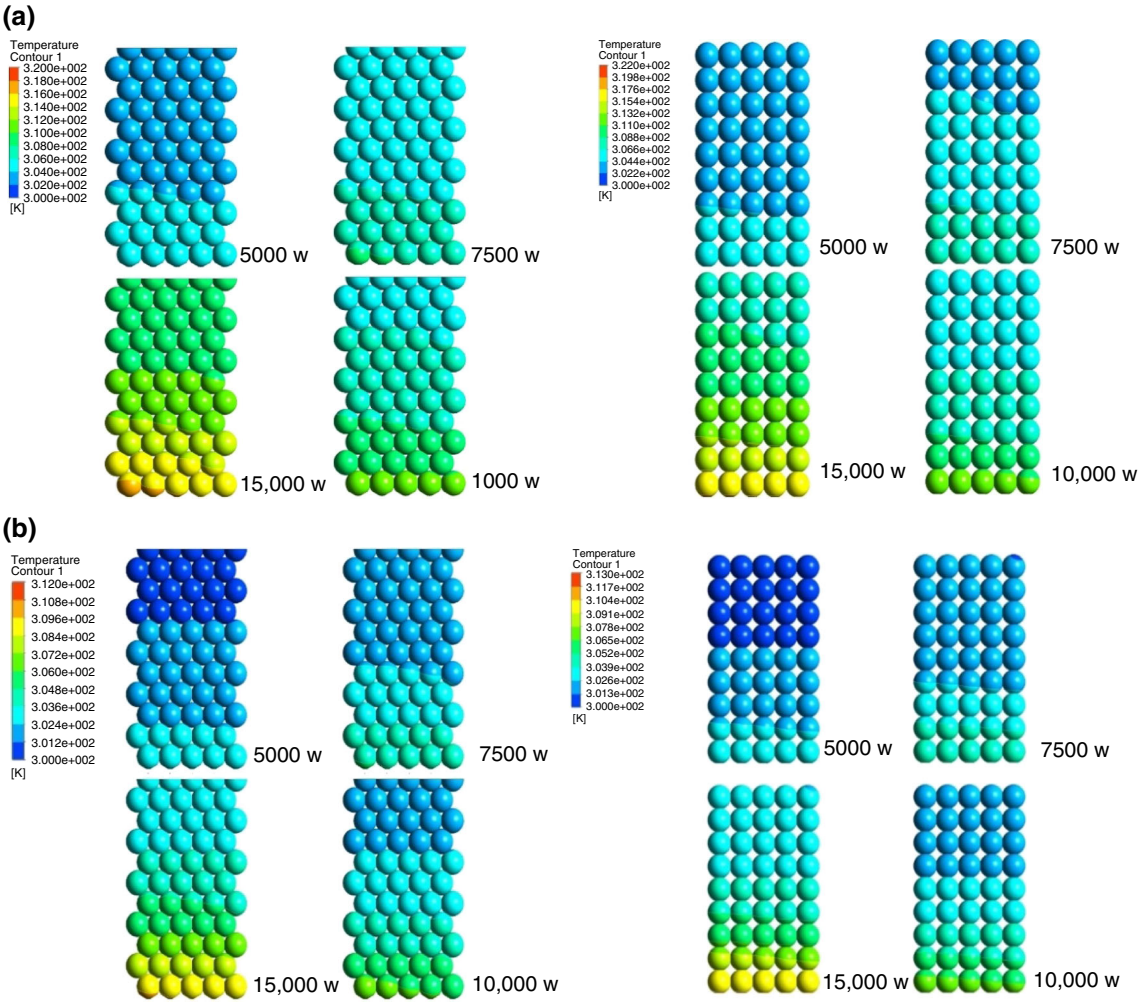

Fig. 15 Temperature contours in the fins in four- and six-contact for the different thermal flux input from the base **a** velocity of 2.5 m s^{-1} and **b** velocity of 10 m s^{-1}

color change over the first four rows of balls in the four-contact model was equivalent to that over the first six rows of balls in the six-contact model. The reason for that is the higher thermal diffusion in the six-contact case rather than that in the four-contact model due to higher number of ball connections in the six-contact case. Figure 16 shows temperature contours for constant fin base temperature boundary conditions at different base temperatures. The results expressed for the constant flux at base (previous figure) hold here as well, but at higher intensities.

Conclusions

In the present research, through a surface analysis and a numerical investigation of sintered fins, the effect of connection type of balls on heat transfer was studied. The main findings can be summarized as follows.

- Surface analysis shows that at constant dimensions of fin, the six-contact connection type provides larger surface area for the fin.
- In the considered fins, it was shown that the six-contact case has a porosity of 33.88%. This is while, in similar conditions, the four-contact connection provided a porosity of 58.88%.
- The results indicated that at the minimum Reynolds number studied in this research, the six-contact fins could enhance heat transfer by about 33% over that of the four-contact case. The increase in heat transfer coefficient in the six-contact fins occurs while these fins tend to develop a higher pressure drop in the passing flow.
- Using six-contact fin instead of four-contact one with similar dimensions lead to 4.355% higher Nusselt number and 3.2% higher fin efficiency.
- Increasing in fin base constant temperature results in decreasing Nusselt number, while enhancement in fin

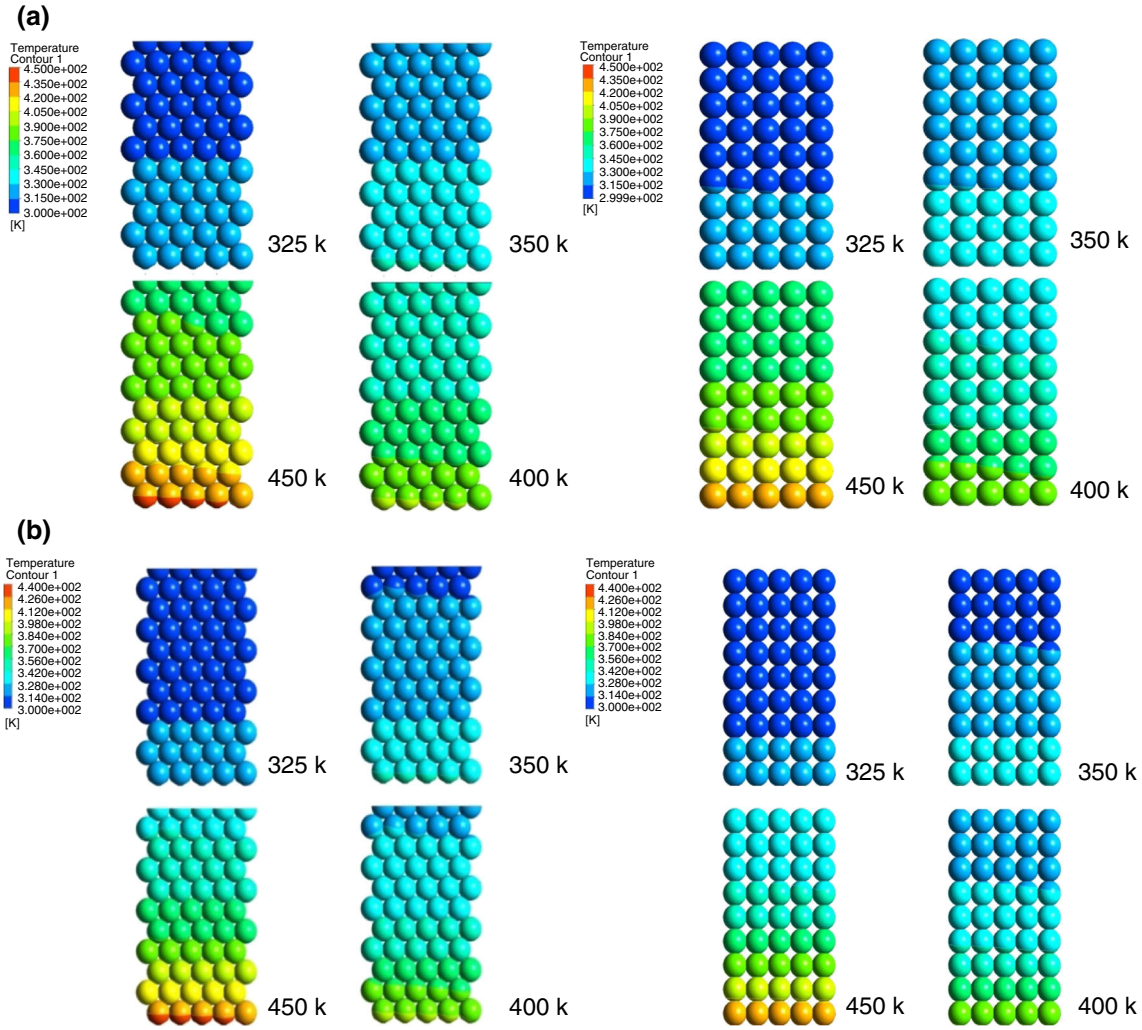

Fig. 16 Temperature contours in the fins in four- and six-contact for the different constant temperature the base **a** velocity of 2.5 m s^{-1} and **b** velocity of 10 m s^{-1}

base constant heat flux leads to Nusselt number augmentation.

References

1. Arpaci VS, Larsen PS. Convection heat transfer. Upper Saddle River: Prentice Hall; 1984.
2. Ye W-B. Enhanced latent heat thermal energy storage in the double tubes using fins. J Therm Anal Calorim. 2017;128(1):533–40.
3. Ben-Nakhi A, Chamkha AJ. Effect of length and inclination of a thin fin on natural convection in a square enclosure. Numer Heat Transf A. 2006;50:381–99.
4. Ben-Nakhi A, Chamkha AJ. Conjugate natural convection around a finned pipe in a square enclosure with internal heat generation. Int J Heat Mass Transf. 2007;50:2260–71.
5. Ben-Nakhi A, Chamkha AJ. Conjugate natural convection in a square enclosure with inclined thin fin of arbitrary length. Int J Therm Sci. 2007;46:467–78.
6. Ben-Nakhi A, Chamkha AJ, Ben Beya B. Effect of inclination on heat transfer and fluid flow in a finned enclosure filled with a dielectric liquid. Numer Heat Transfer, Part A. 2009;56:286–300.
7. Chamkha AJ, Mansour MA, Ahmad SE. Double-diffusive natural convection in inclined finned triangular porous enclosures in the presence of heat generation/absorption effects. Heat Mass Transf. 2010;46:757–68.
8. Ghalambaz M, Jamesahar E, Ismael MA, Chamkha AJ. Fluid-structure interaction study of natural convection heat transfer over a flexible oscillating fin in a square cavity. Int J Therm Sci. 2017;111:256–73.
9. Morega A. Optimal arrays of pin fins and plate fins in laminar forced convection. J Heat Transf. 1993;115:75.
10. Wirtz RA. A semi-empirical model for porous media heat exchanger design. ASME-Publications-Htd. 1997;349:155–62.
11. Jeng T-M, Tzeng S-C. Numerical study of confined slot jet impinging on porous metallic foam heat sink. Int J Heat Mass Transf. 2005;48(23):4685–94.

12. Hamdan M, Al-Nimr MA. The use of porous fins for heat transfer augmentation in parallel-plate channels. Transp Porous Media. 2010;84(2):409–20.
13. Lindstedt M, Karvinen R. Conjugated heat transfer from a uniformly heated plate and a plate fin with uniform base heat flux. Int J Heat Mass Transf. 2017;107:89–95.
14. Bejan A. Entropy generation minimization: the new thermodynamics of finite-size devices and finite-time processes. J Appl Phys. 1996;79(3):1191–218.
15. Chen L, Yang A, Xie Z, Sun F. Constructal entropy generation rate minimization for cylindrical pin-fin heat sinks. Int J Therm Sci. 2017;111:168–74.
16. Alshuraiaan B, Khanafer K. The effect of the position of the heated thin porous fin on the laminar natural convection heat transfer in a differentially heated cavity. Int Commun Heat Mass Transfer. 2016;78:190–9.
17. Bilen K, Gok S, Olcay A, Solmus I. Investigation of the effect of aluminum porous fins on heat transfer. Energy. 2017;138:1187–98.
18. Kundu B, Lee K-S. A proper analytical analysis of annular step porous fins for determining maximum heat transfer. Energy Convers Manag. 2016;110:469–80.
19. Siavashi M, Bahrami HRT, Saffari H. Numerical investigation of flow characteristics, heat transfer and entropy generation of nanofluid flow inside an annular pipe partially or completely filled with porous media using two-phase mixture model. Energy. 2015;93:2451–66.
20. Zargartalebi H, Ghalambaz M, Noghrehabadi A, Chamkha AJ. Natural convection of a nanofluid in an enclosure with inclined local thermal nonequilibrium porous fin considering Buongiorno's model. Numer Heat Transf A. 2016;70:432–45.
21. Vafai K. Handbook of porous media. Boca Raton: CRC Press; 2009.
22. Jiang PX, Li M, Lu TJ, Yu L, Ren ZP. Experimental research on convection heat transfer in sintered porous plate channels. Int J Heat Mass Transf. 2004;47:2085–96.
23. Jiang P-X, Lu X-C. Numerical simulation of fluid flow and convection heat transfer in sintered porous plate channels. Int J Heat Mass Transf. 2006;49(9):1685–95.
24. Chuan L, Wang X-D, Wang T-H, Yan W-M. Fluid flow and heat transfer in microchannel heat sink based on porous fin design concept. Int Commun Heat Mass Transf. 2015;65:52–7.
25. Zhong W, Xu K, Li X, Liao Y, Tao G, Kagawa T. Determination of pressure drop for air flow through sintered metal porous media using a modified Ergun equation. Adv Powder Technol. 2016;27(4):1134–40.
26. Huang G, Zhu Y, Liao Z, Ouyang X-L, Jiang P-X. Experimental investigation of transpiration cooling with phase change for sintered porous plates. Int J Heat Mass Transf. 2017;114:1201–13.
27. Versteeg H-K, Malalasekera W. An introduction to computational Fluid Dynamics: The Finite, vol. Method. London: Pearson Education; 2007.